High-pressure phases of lithium borohydride $LiBH_4$: A first-principles study

Yansun Yao* and Dennis D. Klug
National Research Council of Canada, Ottawa, K1A 0R6, Canada
(Received 6 June 2012; published 15 August 2012)

High-pressure phase transformations in $LiBH_4$ were theoretically investigated using first-principles density functional methods. A series of pressure-induced structural transformations are predicted in $LiBH_4$, as *Pnma* (phase II) → $I4_1/acd$ (phase III) → NaCl type (phase V) → NiAs type (phase VI) → polymeric forms. The calculated pressures for the II → III transition and the III → V transition are 0.9 and 27 GPa, respectively, and both agree very well with recent experimental observations. A B1-B8 transformation becomes more favored at higher pressure, and this results in a distorted NiAs structure of $LiBH_4$. Denoted as phase VI, the distorted NiAs structure is the lowest enthalpy phase of $LiBH_4$ above 60 GPa and confirmed to be dynamically stable by phonon calculations. The ionic character and band gap of the phase VI decreases with increasing pressure. At still higher pressures, the extended structures formed by polymeric BH_4 layers intercalated by $Li^{\delta+}$ cations may exist, and these represent the metallic forms of $LiBH_4$.

DOI: 10.1103/PhysRevB.86.064107 PACS number(s): 61.66.Fn, 61.50.Ks, 71.15.Mb, 71.15.Pd

I. INTRODUCTION

Hydrogen is a promising candidate to eventually replace petroleum as the primary energy source, and extensive scientific effort is being devoted to look for suitable materials for its storage. Various solid-state hydrogen carriers have been investigated, both theoretically and experimentally, including metal hydrides, carbon hydrates, clathrate hydrates, and metal-organic frameworks (MOFs). Recently lithium borohydrides ($LiBH_4$) have attracted increased attention as a possible hydrogen storage medium, owing to its high gravimetric and volumetric hydrogen density, e.g. ∼18.5 wt% of hydrogen.[1–5] In order to use $LiBH_4$ for practical hydrogen storage, however, one of the difficulties is its high thermal stability with respect to hydrogen desorption. As hydrogen binds strongly within the $[BH_4]^{\delta-}$ anions, high temperatures are required to release hydrogen from $LiBH_4$. There have been several approaches to this problem, including the study of binary mixtures of $LiBH_4$ with other hydrogen-rich compounds, such as MgH_2 and $LiNH_2$.[6–9] In these mixtures, the $[BH_4]^{\delta-}$ anions are destabilized via chemical reaction with other hydrides, and therefore the energy costs in hydrogen release can be reduced. A different approach that may be considered is applying extremely high pressure on $LiBH_4$, in order to reduce the H. . . H contacts between $[BH_4]^{\delta-}$ anions and therefore destabilize the B-H bonds.[10–16] This effort will likely decrease the activation energies for hydrogen release in $LiBH_4$. It was further suggested that the high-pressure phases of $LiBH_4$ may be stabilized at ambient pressure by partial substitutions of $Li^{\delta+}/[BH_4]^{\delta-}$ with larger cations/anions and therefore serve as an improved hydrogen storage material.[12]

The study of the high-pressure behaviors of $LiBH_4$ can therefore yield important information about its structural characteristics and perhaps help to understand its desorption dynamics under ambient conditions. Yet, the compression of hydrogen-rich compounds by itself is a fascinating subject in material sciences, as it may yield new pathways to attaining a metallic state of hydrogen.[17–19] One may view the hydrogen in these systems as being chemically precompressed by the heavier atoms, and therefore it requires lower pressure for metallization than that expected for pure hydrogen. As theoretically predicted, one of the interesting aspects of the metallic hydrogen and hydrogen-rich compounds is the possibility of high-T_c superconductivity.[19,20] This prediction makes the investigation of compressed $LiBH_4$ tempting because of its low atomic mass and high hydrogen density that enhance the possibility of strong electron-phonon coupling in the system.

Crystalline $LiBH_4$ has an orthorhombic *Pnma* structure (phase II) at ambient conditions.[21,22] On heating to 381 K, the *Pnma* structure transforms to a high-temperature phase. Based on recent neutron and synchrotron diffraction data, it is generally accepted that the high-temperature phase of $LiBH_4$ has the $P6_3mc$ space group (phase I),[21,23,24] although other candidate structures have also been suggested.[25,26] Upon applying pressure, at least two high-pressure phases of $LiBH_4$ have been characterized from recent synchrotron diffraction studies at room temperature. The high-pressure phase III, observed between 1.2 and 10 GPa, was originally interpreted as an orthorhombic structure with the *Ama*2 space group,[12] but a very recent study argues that this structure belongs to the $I4_1/acd$ space group.[16] With a further increase of the pressure, the phase III slowly transforms to a second high-pressure phase (phase V) over a large pressure span of more than 10 GPa and remains stable up to at least 30 GPa, the highest pressure reached in the experiments up to date. The phase V has been identified by two independent experiments[12,16] as a face-centered cubic (fcc) NaCl structure, in the same type as the α-$NaBH_4$ structure. A tetragonally distorted NaCl structure (phase V′), possibly corresponding to an incomplete structural transformation, has also been observed in the transition from phase III to phase V.[16]

Prior to this study, several theoretical studies have been carried out on the high-pressure behavior of $LiBH_4$.[25,27,28] A major problem these theoretical studies encountered, however, was that the structures of the high-pressure phases of $LiBH_4$ were not yet known at the time. Several structural models have been predicted from theory, for the high-pressure phases of $LiBH_4$, but none of these structures were observed in the experiments carried out thereafter. With the recent discovery of phases III and V in experiments, an updated and hopefully more accurate theoretical study is needed for the high-pressure

behaviors of $LiBH_4$, and this motivates the present study. In this paper, we study the structural stabilities of the observed and proposed structures of $LiBH_4$ using the density functional theory (DFT) method and predict a phase transition sequence of $LiBH_4$ at high pressure. The controversy on the structure of the phase III has been resolved from our study, with the $I4_1/acd$ structure suggested as the correct structure. The calculated pressures of phase transitions using the $I4_1/acd$ structure as the phase III agree well with the experiments. In addition to solving the existing problems in the high-pressure forms of $LiBH_4$, we also take one step further in this study by predicting a new phase of $LiBH_4$ (named as phase VI), which is calculated to be more stable than the NaCl phase V structure above 60 GPa. The predicted phase VI has a distorted NiAs structure. The microscopic mechanism for the phase V-to-phase VI transition (B1-B8) is characterized, in an effort to provide guidance for the future experiments on this interesting subject. We also predict that, with sufficient compression, $LiBH_4$ will eventually reach a metallic phase in polymeric structures constructed by extended BH_4 layers intercalated with $Li^{\delta+}$ cations.

II. COMPUTATIONAL DETAILS

Car–Parrinello molecular dynamics (CPMD) calculations[29] were employed to investigate the high-pressure phase transitions of $LiBH_4$. The NaCl supercell with 384 atoms (64 $LiBH_4$ units) was optimized at different pressures and used as the initial configurations. All CPMD calculations were performed with the Quantum ESPRESSO package (PWSCF).[30] Ultrasoft pseudopotentials were used to describe valence electron-nuclei interactions.[31] The 1*s* electrons are included in the valence of the Li pseudopotential. The generalized gradient approximation (GGA) was employed with a Perdew–Burke–Ernzerhof (PBE) exchange correlation functional.[32] Electronic wave functions and the charge density were expanded in a plane-wave basis set using an energy cutoff of 40 and 240 Ry, respectively. To crosscheck the reliability of the PBE functional, some calculations have been repeated using the local density approximation (LDA).[33] A fictitious electron mass of the electronic wave function of 200 a.u. and a time step of 4 a.u. were used for the time integration of the ionic motions.[34] The Brillouin zone (BZ) sampling was restricted to the zone center. The simulation cell was initially equilibrated for 3 ps to 300 K in a canonical (NVT) ensemble, followed by a pressure equilibration of 8 ps in the isothermal-isobaric (NPT) ensemble. The equilibrated trajectories were then obtained in a microcanonical (NVE) ensemble after an additional temperature equilibration (3 ps) in a canonical (NVT) ensemble to avoid temperature drifting. The temperature in the CPMD calculations was controlled by a Nosé thermostat.[35] Once a phase transition is observed, the supercell is quenched to local energy minimum using structural optimization.

The electronic calculations were performed using the Vienna *ab initio* simulation (VASP) code[36] and projector-augmented plane-wave (PAW) potentials[37,38] with the PBE functional. The 1*s* electrons are included in the valence of the Li potential. A high energy cutoff of 910 eV was used in all calculations. Dense *k*-point grids[39] were employed to sample the first BZ for candidate structures and yield energies that converged to within 1 meV/atom. Specifically, the *k*-point grids used in the total-energy calculations are $6 \times 6 \times 6$ for the $I4_1/acd$ structure, $6 \times 9 \times 6$ for the *Pnma* structures (two in total, see below), $12 \times 12 \times 9$ for the NaCl and $P4_2/nmc$ structures, $12 \times 12 \times 8$ for the hexagonal structure, $6 \times 6 \times 6$ for the distorted NiAs structure, $12 \times 12 \times 8$ for the *Ama*2 structure, and $6 \times 9 \times 6$ for the $P6_3mc$ structure. Phonon calculations for the distorted NiAs structure were performed using the ABINIT program[40] employing the linear response method with Trouiller–Martins norm conserving pseudopotentials[41] and an energy cutoff of 40 Hartree and a $4 \times 4 \times 4$ *k*-point mesh employed on a $2 \times 2 \times 2$ *q*-point mesh.

III. RESULTS AND DISCUSSIONS

The first dense phase of $LiBH_4$, phase III, was observed more than 30 years ago,[10] but its detailed structure is still presently under debate. Several candidate structures have been predicted from theoretical studies, including an $NaBH_4$-type structure above 6.2 GPa,[28] a monoclinic $P2_1/c$ structure above 1 GPa,[27] and a monoclinic Cc structure above 2.2 GPa,[27] but none of these predicted structures corresponds to the phase III characterized in recent synchrotron x-ray diffraction experiments. There are two possible structure models proposed from recent synchrotron experiments, however: an orthorhombic *Ama*2[12] and a tetragonal $I4_1/acd$ structure;[16] both can reasonably fit the x-ray diffraction patterns of the phase III (weak x-ray diffraction of light elements make interpretation of the measurements difficult), and this is presently the source of the controversy.

From the enthalpy calculations [Fig. 1(a)], we found that the $I4_1/acd$ structure becomes more stable than the *Pnma* structure (phase II) at approximately 0.9 GPa. This transition pressure agrees very well with the experimentally determined pressure for the phase II-III transition at $0.8 \sim 1.2$ GPa, strongly suggesting the $I4_1/acd$ structure as the structure of the phase III. The proposed *Ama*2 structure, on the other hand, never becomes more stable than the phase II, and its enthalpy actually becomes increasingly higher than the $I4_1/acd$ structure at high pressures. The calculated energetics therefore eliminates the *Ama*2 structure as the structure of the phase III. The enthalpies of the theoretically predicted structures of the phase III have also been calculated in this pressure region, and none of them was found to be more energetically favorable than the $I4_1/acd$ structure. One point that needs to be mentioned is that another *Pnma* structure has been predicted from theory as the ground state of $LiBH_4$.[26] This *Pnma* structure has an enthalpy very close to the experimentally identified one, and therefore would become less stable than the $I4_1/acd$ structure at a similar transition pressure [Fig. 1(a)]. It should be noted that the calculated enthalpies in Fig. 1(a) essentially describe the ground states at zero temperature. The energy orders of competing structures at finite temperatures are determined by their Gibbs free energies, which may be estimated using the quasiharmonic approximation. In this study, however, the complexity of the $LiBH_4$ structures makes free energy calculations (as a function of pressure) impractical. On the other hand, since all competing structures of $LiBH_4$ have similar bonding patterns, the

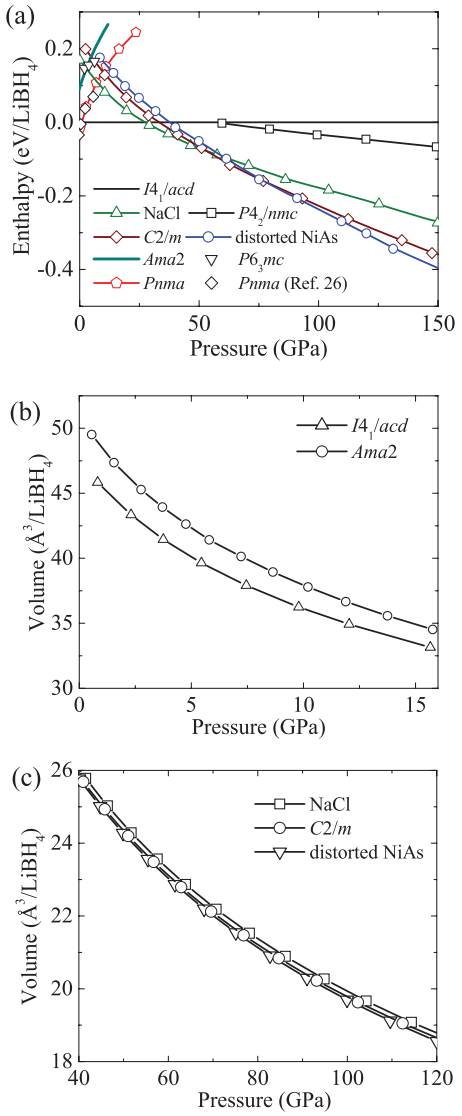

FIG. 1. (Color online) (a) Calculated enthalpies per formula unit for candidate structures of $LiBH_4$ in the pressure range 0–150 GPa. The enthalpies of the $I4_1/acd$ structure are taken as the reference enthalpies. The *Pnma* structure in pentagons is the observed phase II, while the one in diamonds is a predicted structure in Ref. 26. (b) A comparison of the formula volume between the $I4_1/acd$ and *Ama*2 structure in the pressure region 0–16 GPa. (c) A comparison of the formula volume between the NaCl, $C2/m$, and distorted NiAs structure in the pressure region 40–120 GPa.

entropies of these structures should also be similar. Therefore, having the zero-point energies and entropies included may modify the phase transition pressures but would not likely change the order of the transitions.

Based on the enthalpy calculations, we suggest that the $I4_1/acd$ structure is the observed phase III of $LiBH_4$. Despite the large difference in enthalpy, the $I4_1/acd$ and *Ama*2 structures are not significantly different in general (Fig. 2). Both structures can be described by a similar basic motif, with the $Li^{\delta+}$ cations forming a simple cubic (sc) lattice and tetrahedrally coordinated with the $[BH_4]^{\delta-}$ anions. In turn, each $[BH_4]^{\delta-}$ anion is surrounded by a square-planar coordination of four $Li^{\delta+}$ cations, an interesting structural

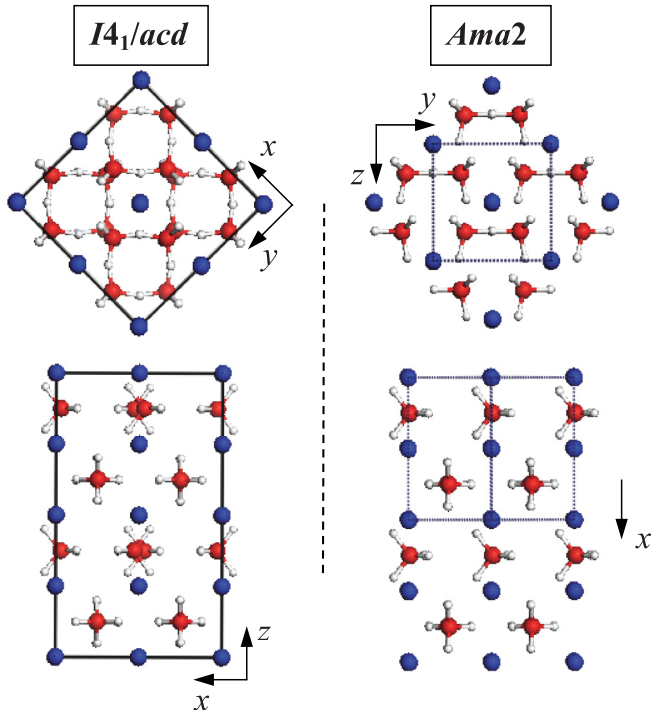

FIG. 2. (Color online) A comparison between the $I4_1/acd$ and *Ama*2 structures in a common cell and viewed from two different directions. The unit cells of the two structures are indicated by solid and dotted lines, respectively.

feature never seen in any other metal borohydrides. Having the same structural motif, the energetic order of the two structures is determined by the local coordination of $Li^{\delta+}$ cations to $[BH_4]^{\delta-}$ anions. The $[BH_4]^-$ ion, as the simplest anionic boron hydride, has the tendency of forming compounds by three-center bonding to metal cations, previously seen, for example, in transition metals, lanthanides, and actinides, and the structural stability of these compounds strongly depends on the local coordination of the metal atoms and on the hydrogen configuration in the BH_4 groups.[42]

Two modes of attachment of the tetrahydroborate ligand to a metal ion, bidentate and tridentate, have been observed previously in metal borohydrides. It was argued that the bidentate ligation is more energetically favorable than the tridentate one for $LiBH_4$. The observed *Pnma* structure of $LiBH_4$ (phase II) has a mixture of bidentate and tridentate configurations. In both *Ama*2 and $I4_1/acd$ structures of $LiBH_4$, only the bidentate ligation pattern is seen [Figs. 3(a) and 3(b)]. The detailed orientations of the $[BH_4]^{\delta-}$ anions, however, are different in the two structures. In the *Ama*2 structure, the hydrogen atoms of four $[BH_4]^{\delta-}$ anions are alternatively eclipsed and staggered with each other. The hydrogen atoms of four $[BH_4]^{\delta-}$ anions in the $I4_1/acd$ structure, on the other hand, are all staggered with each other. The all-staggered hydrogen configuration will minimize the repulsive forces as well as mesh better the $Li^{\delta+}$ cation with four $[BH_4]^{\delta-}$ anions and therefore would be the likely choice for the structure at high pressure.

The two Li-H distances in the $I4_1/acd$ structure, 1.95 and 2.05 Å, are in general shorter than the four Li-H distances in the *Ama*2 structure from 1.96 to 2.14 Å (both calculated at 3.7 GPa), indicating stronger bonding interactions

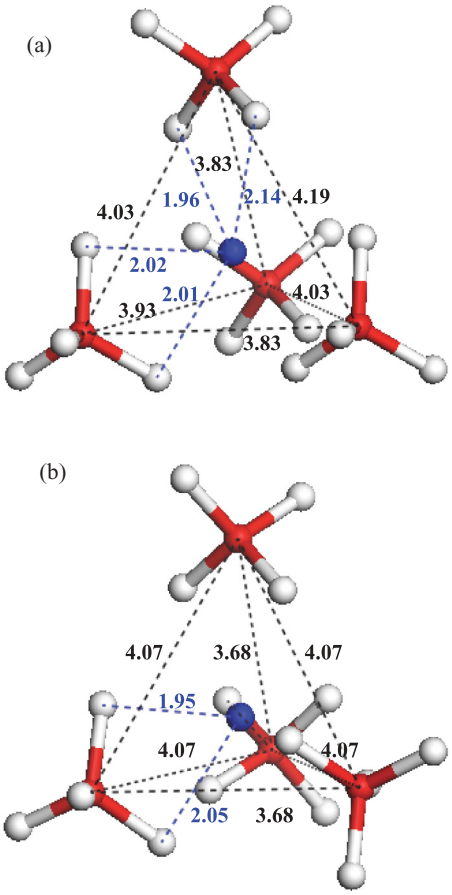

FIG. 3. (Color online) The local structures of $LiBH_4$ for (a) *Ama*2 and (b) $I4_1/acd$ structure. The interatomic distances in Angstroms in the two models are obtained at the same pressure 3.7 GPa.

[Figs. 3(a) and 3(b)]. The four $[BH_4]^{\delta-}$ anions form a distorted tetrahedron with the $Li^{\delta+}$ cation in the void. The all-staggered hydrogen configuration results in a smaller volume for the tetrahedron. The $I4_1/acd$ structure, therefore, always has smaller volume than the *Ama*2 structure in the relevant pressure region [Fig. 1(b)]. The molecular units in Figs. 3(a) and 3(b) represent the building motif for the *Ama*2 and $I4_1/acd$ structure. The all-staggered configuration [Fig. 3(b)] has two more distinct $[BH_4]^{\delta-}$ orientations than the eclipsed-staggered one [Fig. 3(a)], which makes the crystalline unit cell built from the former at least twice as large as the one built from the latter. The unit cell of the $I4_1/acd$ structure is actually four times larger than the unit cell of the *Ama*2 structure. As shown in Fig. 2, the unit cell of the $I4_1/acd$ structure has the same dimensions as a $\sqrt{2} \times \sqrt{2} \times 2$ supercell of the *Ama*2 structure, generated from the latter by a conversion matrix (1, 1, 0),(−1, 1, 0), (0, 0, 2).

With increasing pressure, the NaCl structure becomes increasingly more stable [Fig. 1(a)]. At approximately 27 GPa, the NaCl structure surpasses the $I4_1/acd$ structure to become the most stable phase (phase V). The calculated pressure for this transition agrees well with the experimental data.[12,16] The experimentally observed phase III-V transition spans a rather large pressure range. The phase transition starts at as low a pressure as 10 GPa and reaches completion into the NaCl structure at 30 GPa. In the intermediate range, a tetragonally distorted NaCl structure has also been observed.[16] If each $[BH_4]^{\delta-}$ anion is treated as a unity, the ideal structure of the phase V has a Fm-3m space group. This structural motif is the same as that of the α-$NaBH_4$, in which the alkali metal cations and $[BH_4]^{\delta-}$ anions are octahedrally coordinated to each other. An interesting structural feature of the phase V suggested from previous experiments is that the $[BH_4]^{\delta-}$ anions appear to undergo dynamical distortions, possibly involving reorientational hydrogen jumps and rotational diffusions. This suggestion is consistent with the dynamics of the $[BH_4]^{\delta-}$ anions in the NaCl structure revealed in our CPMD calculations, where the H atoms in all $[BH_4]^{\delta-}$ anions experience large thermal motions and do not have fixed positions.[43] Due to the high degree of molecular mobility, a direct calculation of the enthalpy for the phase V becomes difficult. Static enthalpy calculations have to be made on fixed structural configurations. To work around this, we determined at different pressure ranges the lowest enthalpy hydrogen configurations in the phase V and calculated their enthalpies [Fig. 1(a)]. An exhaustive search scheme for the lowest enthalpy configurations, designed by us and used successfully in determining the γ phase of ammonium borohydride (NH_4BH_4),[44] has been employed. Many possible space groups of the phase V have been examined, including Fm-3m, F-43m, P-42$_1c$, I-4m2, I-42m, $P4_2/nmc$, C2, and Cc, each representing a local energy minimum.

At pressures above 60 GPa, a new structure predicted from our CPMD simulations becomes more stable than the NaCl structure [Fig. 1(a)]. In this structure, the $Li^{\delta+}$ cations and $[BH_4]^{\delta-}$ anions form a distorted NiAs lattice [Figs. 4(a)–4(c)]. We name this structure as the phase VI of $LiBH_4$. The undistorted structure of this new phase can be viewed as a hexagonal close-packed (hcp) lattice of $[BH_4]^{\delta-}$ anions with the $Li^{\delta+}$ cations occupying the octahedral sites [Fig. 4(d)]. If each $[BH_4]^{\delta-}$ anion is treated as a unit, the undistorted structure has a space group $P6_3/mmc$. Through

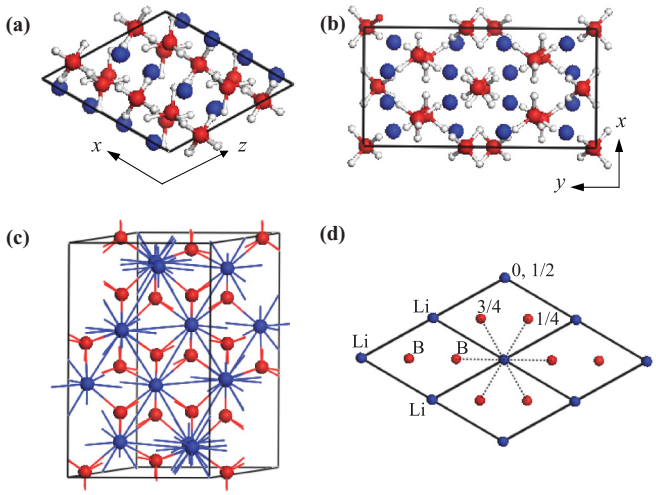

FIG. 4. (Color online) (a) and (b) The predicted phase VI, a distorted NiAs structure, viewed from two different directions. (c) The phase VI shown with the hydrogen atoms removed. The Li and B atoms are located in hexagonal and octahedral sites, respectively. (d) An undistorted NiAs lattice viewed along the *c* axis. The numbers next to the atoms indicate their fractional *z* values in the unit cell.

TABLE I. Structural parameters for the predicted crystalline $LiBH_4$ phases. Unique axis b is used in the setting of space groups for the two monoclinic cells.

Structure (space group)	P (GPa)	Lattice parameters (Å, °)	Atomic coordinates (fractional)			
NiAs ($C2/c$)	100	$a = 6.19$, $b = 10.19$, $c = 5.91$ $\beta = 122.26$	Li 8*f*	0.1271	0.1271	0.5067
			Li 8*f*	0.3702	0.0928	0.0033
			B 8*f*	0.2305	0.2313	0.2023
			B 4*e*	0.0000	0.4333	0.2500
			B 4*e*	0.0000	0.9839	0.2500
			H 8*f*	0.5529	0.2621	0.4911
			H 8*f*	0.4109	0.1277	0.5576
			H 8*f*	0.3472	0.5549	0.2321
			H 8*f*	0.5883	0.4308	0.4524
			H 8*f*	0.3519	0.3213	0.2215
			H 8*f*	0.1676	0.2387	0.3514
			H 8*f*	0.3586	0.1430	0.2419
			H 8*f*	0.1553	0.4985	0.2572
$C2/m$	100	$a = 5.71$, $b = 3.28$, $c = 5.39$ $\beta = 128.52$	Li 2*a*	0.0000	0.0000	0.0000
			Li 2*c*	0.0000	0.0000	0.5000
			B 4*i*	0.4559	0.0000	0.2118
			H 4*i*	0.6975	0.0000	0.0590
			H 4*i*	0.6692	0.0000	0.6863
			H 8*j*	0.6175	0.2707	0.3209

the calculations, we found that the predicted phase VI always has a high packing efficiency (or smaller volume) than phase V [Fig. 1(c)], which makes it a favorable structure at high pressures. A full structural optimization of the phase VI that includes the lowest enthalpy hydrogen orientations yields the $C2/c$ space group. The optimized structural parameters at 100 GPa are listed in Table I. The unit cell of the $C2/c$ configuration contains 16 $LiBH_4$ units (96 atoms).

The phase V and phase VI of $LiBH_4$ are two related structures. In crystal chemistry, the NiAs (B8) structure occupies a unique position. It is one of the most common structures found in AB compounds that contain transition metals and has been considered as being related, on one hand, to the NaCl (B1) structure that is predominately ionic and, on the other hand, to the CsCl (B2) structure that is intermetallic.[45,46] In one of our previous studies, we have found that a similar compound NH_4BH_4 follows the NaCl-CsCl transition sequence under high pressure.[44,47] The structural relation between the phase V and phase VI of $LiBH_4$ is best viewed by comparing the stacking of anion/cation layers along the [111] axis in the NaCl structure [Fig. 5(a)] with the stacking along the c axis in the NiAs structure [Fig. 5(b)]. Both structures are built from alternate anion and cation layers that are parallel to each other. All these layers are identical in shape, formed by an array of equilateral triangles. The only difference between the two structures is the relative positions of the layers. In phase V, the cubic symmetry is maintained, and each type of layer is stacked on three different sites. The stacking pattern for the phase V is ABCDEFABCDEF, with $Li^{\delta+}$ cations and $[BH_4]^{\delta-}$ anions alternatively occupying these sites. The ratio of the distance between neighboring planes to the nearest neighbor distance within the planes is 0.408 for an ideal fcc lattice (analogous to the c/a ratio in hexagonal structures). Both $Li^{\delta+}$ cations and $[BH_4]^{\delta-}$ anions have local octahedral coordination, and

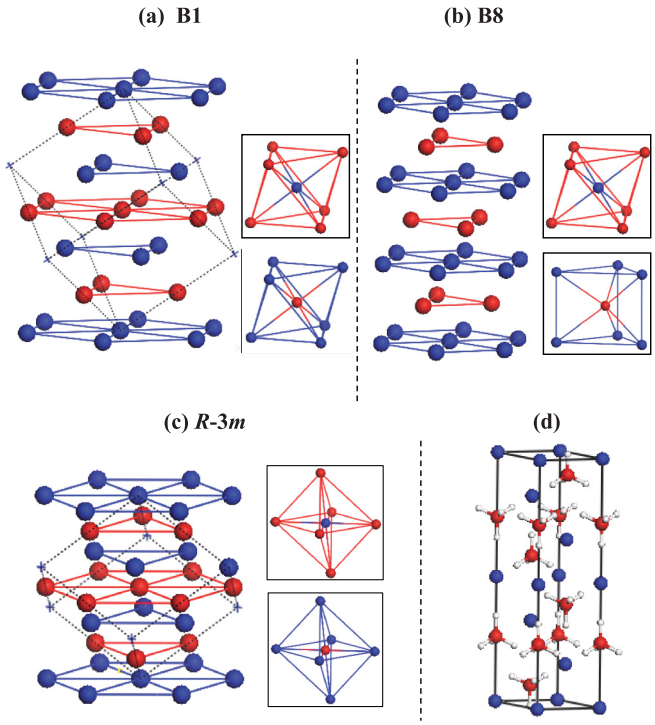

FIG. 5. (Color online) (a) The NaCl structure with the [111] axis of the unit cell (dotted lines) set vertical. (b) The NiAs structure with the c axis set vertical. The Li atoms form a hexagonal lattice, and the B atoms occupy the octahedral sites. (c) The R-3m structure produced by reducing the c/a ratio in the NaCl structure. In (a)–(c), hydrogen atoms are removed from the structures for a clearer presentation, and the stacking sequence of atoms occupying the layers is Li-B-Li-B-Li-B-Li. The local $Li[BH_4]_6$ and Li_6BH_4 structures are shown in the upper and lower frames of the insets, respectively, with hydrogen atoms removed for clarity. (d) The R-3m structure with a guessed hydrogen arrangement shown in the hexagonal setting.

therefore their locations are interchangeable. The Li_6BH_4 and $Li[BH_4]_6$ octahedrons are displayed in Fig. 5(a).

The transition from the phase V to the phase VI involves relative shifts of neighboring planes and the change of the c/a ratio. The stacking pattern for the phase VI is ABACABAC, with $Li^{\delta+}$ cations on A sites and $[BH_4]^{\delta-}$ anions on B and C sites [Fig. 5(b)]. The phase V-to-phase VI transition does not change the local coordination of anions around each cation—six $[BH_4]^{\delta-}$ anions are still arranged around each $Li^{\delta+}$ cation to form an $Li[BH_4]_6$ octahedron. The local coordination of cations around each anion, however, changes completely after the transition. In phase VI, six $Li^{\delta+}$ cations are arranged around the central $[BH_4]^{\delta-}$ anion and from a Li_6BH_4 trigonal prism, instead of the Li_6BH_4 octahedron in phase V. The preference of Li_6BH_4 trigonal prisms in the phase VI may suggest increasingly attractive interactions among $Li^{\delta+}$ cations at high pressures. Originally predicted by Neaton and Ashcroft, light alkali metals have the tendency of forming paired ground states at high pressures, a compelling feature similar to molecular hydrogen.[48] In the Li_6BH_4 octahedron, the top Li_3 equilateral triangle is rotated to a position of having maximum Li-Li separations to the bottom equilateral triangle [Fig. 5(a)]. This orientation is favored when the second-nearest neighbors, in this case $Li^{\delta+}$ cations, strongly repel each other. On the other hand, in the Li_6BH_4 trigonal prism, the top Li_3 equilateral triangle is directly on top of the bottom equilateral triangle, resulting in shorter Li-Li separations [Fig. 5(b)]. This orientation is preferred when $Li^{\delta+}$ cations have attractive interactions with each other. The predicted phase VI of $LiBH_4$ is dynamically stable in the high-pressure region, as indicated by the absence of imaginary phonon frequencies in the calculated phonon dispersions.[43]

We note that we have also considered another possible way to transform the phase V of $LiBH_4$ into a new structure—by decreasing the c/a ratio only. This distortion will result in a rhombohedral structure. Treating each $[BH_4]^{\delta-}$ anion as a unity, the structure has the R-3m space group [Fig. 5(c)]. This consideration is inspired by our previous study of high-pressure behaviors of the molecular compound $SiH_4(H_2)_2$, in which a similar rhombohedral distortion of the fcc lattice formed by SiH_4 groups has been predicted at increasing pressure.[49] In this structure, both cations and anions have the same distorted octahedral coordination, and therefore their locations are interchangeable. A guessed model of the rhombohedral structure with hydrogen included in the unit cell is shown in Fig. 5(d) (structure is shown in hexagonal setting). We have examined numerous guessed structures in this model and found several energy minima. The lowest energy structure in this group of structures, after a full structural optimization, distorts to the $C2/m$ space group (Table I). The $C2/m$ structure is competitive in enthalpy with the phase VI in a large pressure range approximately from 50 to 90 GPa and then becomes less stable than the latter [Fig. 1(a)]. It also has slightly larger volume than the phase VI [Fig. 1(c)]. This structure might therefore correspond to a metastable phase of $LiBH_4$.

The $Li^{\delta+}$ cations and $[BH_4]^{\delta-}$ anions in the phase VI have more confined motions than in the phase V. In phase VI, the $Li^{\delta+}$ cations and $[BH_4]^{\delta-}$ anions remain fixed at their original locations and undergo thermal vibrations.[43] The dynamical

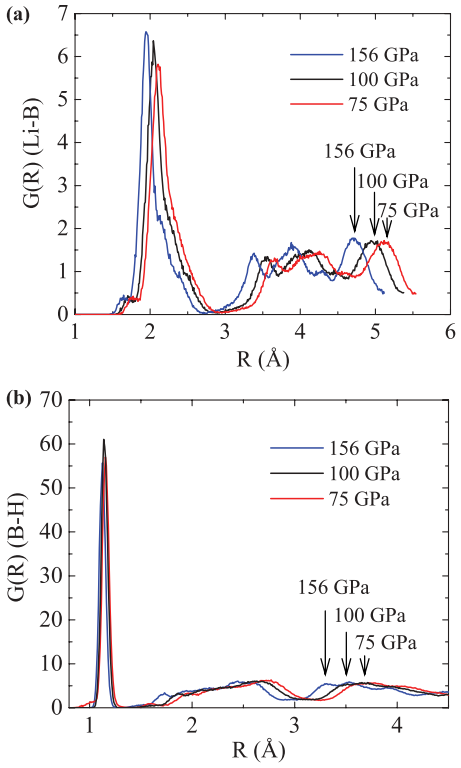

FIG. 6. (Color online) The radial distribution functions for (a) Li-B and (b) B-H, calculated from the CPMD trajectories of the phase VI at three pressures.

distortions of the $[BH_4]^{\delta-}$ anions are still notable in the phase VI, but the reorientational hydrogen jumps, and rotational diffusions do not exist anymore, and the planes maintain a basic hexagonal shape. This finding is not exactly surprising since, at higher pressure, the enhanced interactions with $Li^{\delta+}$ cations will reduce the mobility of the $[BH_4]^{\delta-}$ anions, in particular the rotation modes. The increased cation-anion interactions can be viewed from the radial distribution function $G(r)$ for Li-B separations, calculated for the phase VI from the CPMD trajectories at three different pressures [Fig. 6(a)]. The first peak, corresponding to the nearest neighbor distances between Li and B, decrease from 2.12 to 1.94 Å in a pressure range of 80 GPa. The second and third nearest neighbor distances decrease even more substantially by 0.37 and 0.42 Å, respectively. On the other hand, the distances between bonded boron and hydrogen atoms within each $[BH_4]^{\delta-}$ anion do not have notable changes in this pressure region [Fig. 6(b)]. The first peak of the B-H radial distribution function, corresponding to the B-H bonds, calculated at three pressures, is all located at about 1.16 Å. This B-H separation does not differ much from that of the equilibrated B-H distance at ambient conditions, e.g. 1.19 Å measured from the B-H terminal bonds in a diborane molecule.[50] The H-B-H bond angles, on the other hand, are distorted from the ideal value in the T_d symmetry (109.5°) into a range of 103.4°–121.5° at 75 GPa.

The predicted phase VI of $LiBH_4$ is still an insulating phase. The bonding nature within the $[BH_4]^{\delta-}$ anion is predominately covalent, which is stabilized by the electron transferred from nearby Li atoms. The electronic density of states (DOS) of the phase VI calculated at 75 GPa is shown in Fig. 7. A large

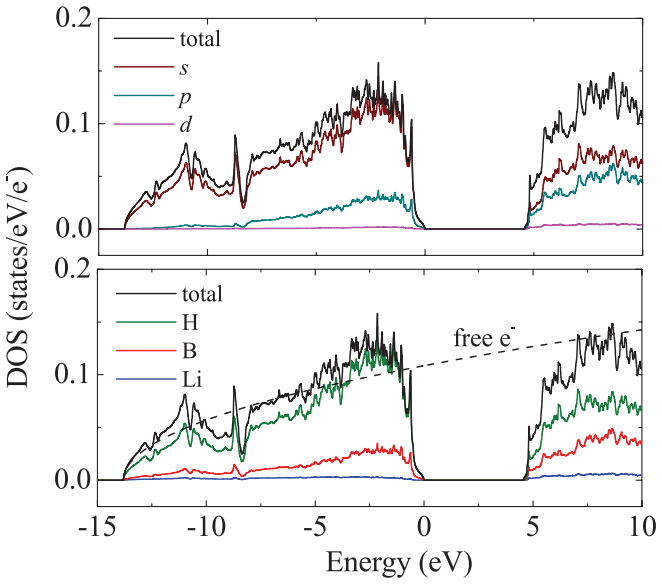

FIG. 7. (Color online) Total electronic DOS of the phase VI and its projections to different elements and wave functions calculated at 75 GPa. The DOS of free electrons is also shown for comparison (dashed curve). The projected DOS follows the descending order from total, s, p, d in the upper frame and total, H, B, Li in lower frame.

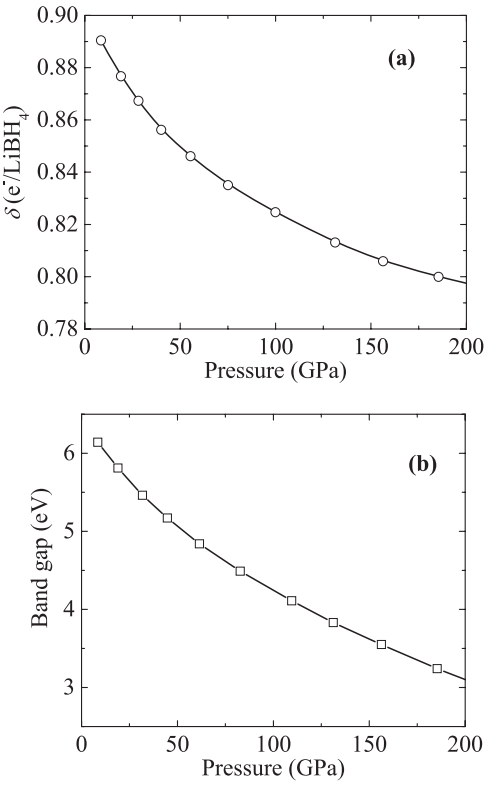

FIG. 8. (a) Charge transfer δ from Li to BH_4 group and (b) magnitude of band gap in the phase VI as functions of pressure.

energy gap of nearly 4.6 eV appears between the valence and conduction bands. The valence bands span an energy range from −13.8 to 0 eV (Fermi level). The entire valence DOS is dominated by the s electrons of the H atoms. The boron DOS mixes strongly with the hydrogen DOS throughout the valence regime and contributes to the sp^3 hybridization that is a prerequisite for the formation of BH_4 tetrahedron. The contribution from the d electrons, on the other hand, is negligible. The s and p electrons on the B atoms are mainly located in energy regimes below and above −8.4 eV, respectively. Here, we note the similarity of the valence DOS in the low-energy regime to that of the free electrons. The contribution from the Li atoms to the total DOS is hardly seen in the valence regime, indicating that electrons are almost depleted from the $2s$ orbital at this point.

With increasing the pressure, electrons start moving back from the anions to the cations, and the ionicity of the $LiBH_4$ compounds decreases. To demonstrate this, we have calculated at different pressures the Bader charges[51,52] for each component in the phase VI of $LiBH_4$. Using the calculated Bader charges, we derived the amount of charge transfer δ from Li to the BH_4 group at different pressures [Fig. 8(a)]. At the low end of the chosen pressure region, i.e. 8.48 GPa, the δ is approximately 0.9 e^- per each $LiBH_4$ unit. At 185 GPa, the δ reduces to less than 0.8 e^- per each $LiBH_4$ unit, indicating a weakening in the ionic bonding. The reduced ionicity at high pressures destabilizes the sp^3 bonding and increases the metallicity in $LiBH_4$. As shown in Fig. 8(b), the calculated band gap in the phase VI also reduces substantially in this pressure region, from 6.14 to 3.11 eV, following a tendency toward reaching a metallic state. It should, of course, be emphasized that the present DFT results reflect the usual underestimation of these band gap values.

At still higher pressures, one expects that the phase VI of $LiBH_4$ will transform to other (undiscovered) phases. We have not yet investigated the detailed structures of these phases but might speculate that, by sufficient compression, the $[BH_4]^{\delta-}$ anions will reach more compact forms, possibly through dimerization (B_2H_8) or/and polymerization process ($B_\infty H_\infty$). The molecular forms of $LiBH_4$ studied so far, as pressure increases, will eventually be replaced by extended polymeric networks. We might also suggest that the $[BH_4]^{\delta-}$ polymers should have a similar local structural motif to polymeric alane[53] or borane,[54,55] and form either one-dimensional chains or two-dimensional layers that are intercalated by $Li^{\delta+}$ cations. We have considered several trial models of $[BH_4]^{\delta-}$ polymers and examined their structural stabilities. One structure was constructed from the analogy with the pentacoordinated B_3H_9 trimer motif,[56] in which the B atoms are linked together by bridging H atoms, through three-center two-electron (3c-2e) bonds, and form a layer of zigzag chains that are intercalated with parallel planes of $Li^{\delta+}$ cations. Each B atom in these chains is connected to two bridging H atoms and three terminal H atoms that are alternately above and below the chain. After a full structural optimization, the layer of zigzag chains distort spontaneously to a ragged sheet of B atoms, connected alternately by B-H-B and B-B linkages. The optimized structure has the $C2/m$ space group, denoted as the polymeric $C2/m$ structure (for details, see supplementary material[43]). The B atoms in the polymeric $C2/m$ structure are seven coordinated, similar to the structural motif of a tetraprotonated B_2H_8.[57] Notably, the polymeric $C2/m$ structure is not only a local energy minimum, but also becomes more stable than the phase

VI above 425 GPa,[43] strongly supporting the suggestion that polymeric structures may form in $LiBH_4$ by compression. The polymeric $C2/m$ structure, being metallic by its construction, represents a variety of polymeric forms of $LiBH_4$ at extreme pressures. In the metallic state of $LiBH_4$, the large hydrogen density enhances the possibility of strong electron-phonon coupling associated with the vibrations of H atoms, which is promising for enhanced superconductivity behavior. The present results therefore encourage further experimental study of $LiBH_4$ at high pressure.

IV. CONCLUSIONS

High-pressure phase transitions of $LiBH_4$ have been theoretically investigated using the pseudopotential plane-wave method based on density functional theory. The controversy regarding the structure of high-pressure phase III of $LiBH_4$ has been resolved, with the tetragonal $I4_1/acd$ structure suggested as the correct structure. The pressure-induced structural transformations in $LiBH_4$ are predicted as $Pnma$ (phase II) $\rightarrow$ $I4_1/acd$ (phase III) $\rightarrow$ NaCl type (phase V) $\rightarrow$ NiAs type (phase VI) $\rightarrow$ polymeric forms. The phase VI has been predicted in this study using the Car–Parrinello molecular dynamics simulations starting from the phase V at higher pressures. The microscopic mechanisms for the phase V-to-phase VI transition (B1-B8) are characterized. It is found that the atomic mobility in the phase VI is greatly reduced compared with that in the phase V. With increasing pressure, the ionicity of the phase VI decreases, and the band gap reduces toward the formation of a metallic state. At still higher pressure, the polymeric (and possibly metallic) structures will replace molecular structures to become the most stable phases of $LiBH_4$.

*Corresponding author: Yansun.Yao@nrc.ca

[1] S. Orimo, Y. Nakamori, J. R. Eliseo, A. Züttel, and C. M. Jensen, Chem. Rev. **107**, 4111 (2007).
[2] A. Züttel, A. Borgschulte, and S. Orimo, Scr. Mater. **56**, 823 (2007).
[3] B. Sakintuna, F. Lamari-Darkrim, and M. Hirscher, Int. J. Hydrogen Energy **32**, 1121 (2007).
[4] L. George and S. K. Saxena, Int. J. Hydrogen Energy **35**, 5454 (2010).
[5] I. P. Jain, P. Jain, and A. Jain, J. Alloys Compd. **503**, 303 (2010).
[6] F. E. Pinkerton, G. P. Meisner, M. Meyer, M. Balogh, and M. Kundrat, J. Phys. Chem. B **109**, 6 (2005).
[7] J. Vajo and S. Skeith, J. Phys. Chem. B **109**, 3719 (2005).
[8] M. Aoki, K. Miwa, T. Noritake, G. Kitahara, Y. Nakamori, S. Orimo, and S. Towata, Appl. Phys. A **80**, 1409 (2005).
[9] J. Yang, A. Sudik, D. J. Siegel, D. Halliday, A. Drews, R. O. Carter, C. Wolverton, G. J. Lewis, J. W. A. Sachtler, J. J. Low, S. A. Faheem, D. A. Lesch, and V. Ozolins, Angew. Chem., Int. Ed. Engl. **47**, 882 (2008).
[10] C. W. F. T. Pistorius, Z. Phys. Chem. Neue Folge **88**, 253 (1974).
[11] A. V. Talyzin, O. Andersson, B. Sundqvist, A. Kurnosov, and L. Dubrovinsky, J. Solid State Chem. **180**, 510 (2007).
[12] Y. Filinchuk, D. Chernyshov, A. Nevidomskyy, and V. Dmitriev, Angew. Chem., Int. Ed. Engl. **47**, 529 (2008).
[13] V. Dmitriev, Y. Filinchuk, D. Chernyshov, A. V. Talyzin, A. Dzwilewski, O. Andersson, B. Sundqvist, and A. Kurnosov, Phys. Rev. B **77**, 174112 (2008).
[14] B. Sundqvist and O. Andersson, Int. J. Thermophys. **30**, 1118 (2009).
[15] H. Takamura, Y. Kuronuma, H. Maekawa, M. Matsuo, and S. Orimo, Solid State Ionics **192**, 118 (2010).
[16] S. Nakano, H. Fujihisa, H. Yamawaki, Y. Gotoh, and T. Kikegawa, Rev. High Pressure Sci. Technol. **21**, 213 (2011).
[17] J. J. Gilman, Phys. Rev. Lett. **26**, 546 (1971).
[18] N. W. Ashcroft, J. Phys.: Condens. Matter **16**, S945 (2004).
[19] N. W. Ashcroft, Phys. Rev. Lett. **92**, 187002 (2004).
[20] N. W. Ashcroft, Phys. Rev. Lett. **21**, 1748 (1968).
[21] J.-Ph. Soulié, G. Renaudin, R. Černy, and K. Yvon, J. Alloys Compd. **346**, 200 (2002).
[22] A. Züttel, S. Rentsch, P. Fischer, P. Wenger, P. Sudan, Ph. Mauron, and Ch. Emmenegger, J. Alloys Compd. **356–357**, 515 (2003).
[23] M. R. Hartman, J. J. Rush, T. J. Udovic, R. C. Bowman, Jr., and S. J. Hwang, J. Solid State Chem. **180**, 1298 (2007).
[24] Y. Filinchuk, D. Chernyshov, and R. Cerny, J. Phys. Chem. C **112**, 10579 (2008).
[25] Z. Łodziana and T. Vegge, Phys. Rev. Lett. **93**, 145501 (2004).
[26] A. Tekin, R. Caputo, and A. Züttel, Phys. Rev. Lett. **104**, 215501 (2010).
[27] T. J. Frankcombe, G. J. Kroes, and A. Züttel, Chem. Phys. Lett. **405**, 73 (2005).
[28] P. Vajeeston, P. Ravindran, A. Kjekshus, and H. Fjellvåg, J. Alloys Compd. **387**, 97 (2005).
[29] R. Car and M. Parrinello, Phys. Rev. Lett. **55**, 2471 (1985).
[30] P. Giannozzi, S. Baroni, N. Bonini, M. Calandra, R. Car, C. Cavazzoni, D. Ceresoli, G. L. Chiarotti, M. Cococcioni, I. Dabo, A. D. Corso, S. de Gironcoli, S. Fabris, G. Fratesi, R. Gebauer, U. Gerstmann, C. Gougoussis, A. Kokalj, M. Lazzeri, L. Martin-Samos, N. Marzari, F. Mauri, R. Mazzarello, S. Paolini, A. Pasquarello, L. Paulatto, C. Sbraccia, S. Scandolo, G. Sclauzero, A. P. Seitsonen, A. Smogunov, P. Umari, and R. M. Wentzcovitch, J. Phys.: Condens. Matter **21**, 395502 (2009).
[31] D. Vanderbilt, Phys. Rev. B **41**, 7892 (1990).
[32] J. P. Perdew, K. Burke, and M. Ernzerhof, Phys. Rev. Lett. **77**, 3865 (1996).
[33] D. M. Ceperley and B. J. Alder, Phys. Rev. Lett. **45**, 566 (1980); ametrized by J. P. Perdew and A. Zunger, Phys. Rev. B **23**, 5048 (1981).
[34] P. Tangney and S. Scandolo, J. Chem. Phys. **116**, 14 (2002).
[35] S. Nosé, Mol. Phys. **52**, 255 (1984).
[36] G. Kresse and J. Hafner, Phys. Rev. B **47**, 558 (1993).
[37] P. E. Blöchl, Phys. Rev. B **50**, 17953 (1994).
[38] G. Kresse and D. Joubert, Phys. Rev. B **59**, 1758 (1999).
[39] H. J. Monkhorst and J. D. Pack, Phys. Rev. B **13**, 5188 (1976).
[40] X. Gonze, J. M. Beuken, R. Caracas, F. Detraux, M. Fuchs, G. M. Rignanese, L. Sindic, M. Verstraete, G. Zerah, F. Jollet, M. Torrent, A. Roy, M. Mikami, Ph. Ghosez, J. Y. Raty, and D. C. Allan, Comput. Mater. Sci. **25**, 478 (2002).
[41] N. Troullier and J. L. Martins, Phys. Rev. B **43**, 1993 (1991).

[42]T. J. Marks and J. R. Kolb, Chem. Rev. **77**, 263 (1977).
[43]See Supplemental Material at http://link.aps.org/supplemental/10.1103/PhysRevB.86.064107 for thermal trajectories of the phases V and VI, phonon dispersions for the phase VI, structural parameters and enthalpies of the predicted polymeric structure.
[44]R. Flacau, Y. Yao, D. D. Klug, S. Desgreniers, and C. I. Ratcliffe, Phys. Chem. Chem. Phys. **14**, 7005 (2012).
[45]A. Cornish, J. Acta Metall. **6**, 371 (1958).
[46]W. Tremel, R. Hoffmann, and J. Silvestre, J. Am. Chem. Soc. **108**, 5174 (1986).
[47]R. Flacau, C. I. Ratcliffe, S. Desgrenier, Y. Yao, D. D. Klug, P. Pallister, I. L. Moudrakovski, and J. A. Ripmeester, Chem. Commun. **46**, 9164 (2010).
[48]J. B. Neaton and N. W. Ashcroft, Nature **400**, 141 (1999).
[49]Y. Yao and D. D. Klug, Proc. Natl. Acad. Sci. USA **107**, 20893 (2010).
[50]H. W. Smith and W. N. Lipscomb, J. Chem. Phys. **43**, 1060 (1965).
[51]R. F. W. Bader, *Atoms in Molecules—A Quantum Theory* (Oxford University Press, Oxford, 1990).
[52]W. Tang, E. Sanville, and G. Henkelman, J. Phys.: Condens. Matter **21**, 084204 (2009).
[53]Y. Liu, J. Hu, G. Wu, Z. Xiong, and P. Chen, J. Phys. Chem. C **111**, 19161 (2007).
[54]K. Abe and N. W. Ashcroft, Phys. Rev. B **84**, 104118 (2011).
[55]Y. Yao and R. Hoffmann, J. Am. Chem. Soc. **133**, 21002 (2011).
[56]B. J. Duke, C. Liang, and H. F. III. Schaefer, J. Am. Chem. Soc. **113**, 2884 (1991).
[57]G. A. Olah, G. K. Surya Prakash, and G. Rasul, Proc. Natl. Acad. Sci. USA **109**, 6825 (2012).